

Vacancy localization in the square dimer model

J. Bouttier,^{1,*} M. Bowick,^{1,2,†} E. Guitter,^{1,‡} and M. Jeng^{2,§}

¹*Service de Physique Théorique, CEA/DSM/SPHT, Unité de recherche associée au CNRS, CEA/Saclay, 91191 Gif sur Yvette Cedex, France*

²*Physics Department, Syracuse University, Syracuse, New York 13244-1130, USA*

(Received 15 June 2007; published 30 October 2007)

We study the classical dimer model on a square lattice with a single vacancy by developing a graph-theoretic classification of the set of all configurations which extends the spanning tree formulation of close-packed dimers. With this formalism, we can address the question of the possible motion of the vacancy induced by dimer slidings. We find a probability $57/4 - 10\sqrt{2}$ for the vacancy to be strictly jammed in an infinite system. More generally, the size distribution of the domain accessible to the vacancy is characterized by a power law decay with exponent $9/8$. On a finite system, the probability that a vacancy in the bulk can reach the boundary falls off as a power law of the system size with exponent $1/4$. The resultant weak localization of vacancies still allows for unbounded diffusion, characterized by a diffusion exponent that we relate to that of diffusion on spanning trees. We also implement numerical simulations of the model with both free and periodic boundary conditions.

DOI: [10.1103/PhysRevE.76.041140](https://doi.org/10.1103/PhysRevE.76.041140)

PACS number(s): 05.50.+q, 02.10.Ox, 68.55.Ln

I. INTRODUCTION

A. The problem

The statistical mechanics of rigid dimers arranged on a lattice is relevant to many physical systems and has appeared repeatedly in the literature over the years. The study of dimer models can shed light on diatomic gases, the thermodynamics of adsorbed films [1], and the classical limit of resonating valence bond (RVB) models of high-temperature superconductivity [2].

The case of close-packed dimers on planar lattices is exactly solvable and the associated mathematical techniques have proven very powerful [3–8]. It provides a paradigm of a geometrically constrained statistical system with a strong interplay between the physical degrees of freedom and the symmetry of the underlying lattice.

New challenges appear if we extend the close-packed dimer models by allowing for defects in the form of vacancies, namely, sites not covered by dimers [7,9–11]. The presence of defects allows dynamical moves for dimers by sliding them into empty sites, as illustrated in Fig. 1. This, in turn, induces motion of the vacancies in the form of discrete jumps, each by two lattice spacings. It is of great interest to characterize as explicitly as possible the nature of the constrained dynamics of vacancies as a model glassy system. In particular, we would like to determine the extent to which a vacancy can diffuse, both spatially and temporally.

In this paper, we consider the simplest case of an isolated vacancy in a sea of dimers on the square lattice. Our primary interest is the structure of the space accessible to the vacancy. In particular, we address the question of whether or not the vacancy is localized, namely, confined to a finite

region. We find that our model exhibits localization but in a very weak form. Although the motion of the vacancy in a fixed dimer background is localized to a finite domain, the mean size of this domain nevertheless diverges upon averaging over all possible dimer backgrounds. We call this property “weak localization,” as it allows vacancies to diffuse arbitrarily far on average. It is also important to investigate the kinetics of vacancy diffusion. We find an anomalous diffusion exponent determined both by the internal structure of the space available to the vacancy and the effects of weak localization which control the size of this space.

B. Outline and summary of results

Our paper is structured as follows. In Sec. II, we recast our dimer problem with a single vacancy as a model of spanning graphs on a rectangular grid by extending a famous construction by Temperley. This construction is recalled in Sec. II A and provides a bijection between dimer configurations with the vacancy on the boundary of the grid and spanning trees on a subgrid. The generalization of this construction, in Sec. II B, to a vacancy in the bulk leads to more general spanning webs, consisting of a central tree component on which the vacancy can freely diffuse, surrounded by

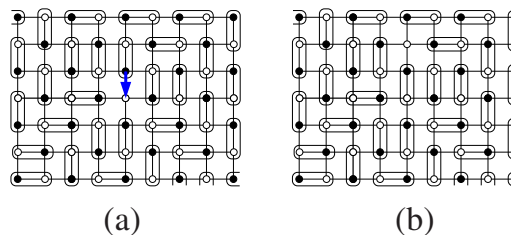


FIG. 1. (Color online) An example of a dimer move on the square lattice. The dimer slides into the empty site (vacancy) configuration (a), resulting in a new configuration (b) where the vacancy has jumped by two lattice spacings.

*jeremie.bouttier@cea.fr

†bowick@phy.syr.edu

‡emmanuel.guitter@cea.fr

§mjeng@phy.syr.edu

a number of nested loops with branches, which act as cages for the vacancy. We then derive in Sec. II C a determinant formula for the partition function of these spanning webs.

Section III is devoted to a finite size study of dimers on a square grid of size L , with a vacancy at the center, and the asymptotic limit $L \rightarrow \infty$. In Sec. III A, we use our determinant formula to compute the probability that the vacancy can reach the boundary of the grid, in which case it can reach all sites of the grid. This “delocalization probability” is found to decay with the system size as $L^{-1/4}$. In Sec. III B, we analyze the distribution $p(s)$ for the size s of the domain accessible to the vacancy in an infinite system. In the spanning web formulation, this domain is nothing but the central tree component that contains the vacancy. We characterize $p(s)$ by first giving the exact value of $p(1)$, which measures the probability that the vacancy is strictly jammed. We then derive its large s behavior $p(s) \sim s^{-9/8}$ from the associated scaling of the delocalization probability. This power law behavior with an exponent larger than -2 is responsible for the announced weak localization property. We finally discuss in Sec. III C the diffusion exponent on spanning webs (η) and on spanning trees (η_0) and find the relation $\eta/\eta_0=7/8$, which measures the slowing of diffusion by weak localization.

We complete our analysis in Sec. IV by a number of numerical simulations both on the statistics of spanning webs and the dynamics of diffusion. In Sec. IV A, we show how to modify the well known Propp-Wilson algorithm for the generation of random spanning trees so as to obtain spanning webs with a uniform measure. We present results for the delocalization probability and for the size distribution $p(s)$, finding good agreement with the analytic predictions. We check the universality of $p(s)$ by also carrying out simulations with periodic boundary conditions. There we used the efficient “pivot algorithm” to generate configurations directly in the dimer formulation. Section IV B is devoted to the numerical computation of the diffusion exponents η_0 on spanning trees and η on spanning webs, whose ratio agrees with the analytic prediction.

Appendix A gives a heuristic derivation of the decay exponent for the delocalization probability via Coulomb gas arguments. Appendix B discusses the technical details of the extension of the Propp-Wilson algorithm to the generation of spanning webs.

II. VACANCY IN A DENSE SEA OF DIMERS: GRAPH-THEORETIC TREATMENT

A. Tree formulation

Let us first recall Temperley’s bijection between dimer configurations on a rectangular grid and spanning trees on a grid with double mesh size [12,13]. More precisely, let us consider a rectangular grid with $2L+1$ columns and $2M+1$ rows, so that the total number of vertices is odd. The vertices of the grid can be colored, say in black and white, so that neighboring vertices have different colors, with the vertex in the upper right corner being white. With this coloring, there is one more white vertex than black vertex and the grid can

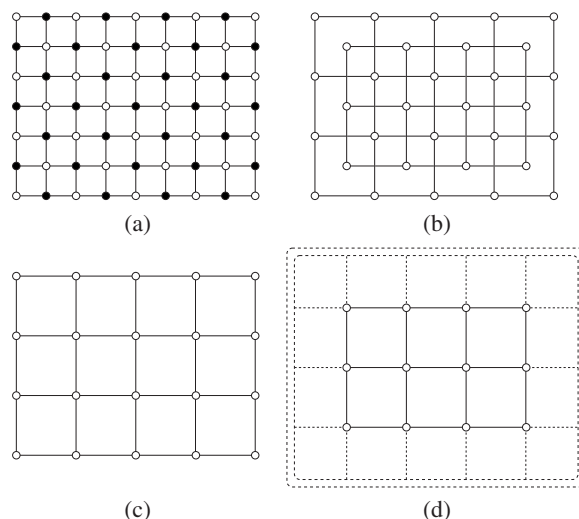


FIG. 2. A 9×7 grid (a) is bicolored with one more white than black vertex. The set of white vertices is made of two intercalated grids of double mesh size (b) with respective sizes 5×4 and 4×3 . The first one (c) will be referred to as the odd white grid and the second one (d) as the even white grid. The latter is extended (dashed lines) so as to include an extra vertex (here represented by a double boundary) dual to the exterior face.

be fully covered by a set of dimers with a single vacancy on a white vertex. Note that the set of white vertices can be viewed as made of two intercalated grids of size $(L+1) \times (M+1)$ and $L \times M$, respectively, both with double mesh size (see Fig. 2). We shall refer to these grids as the odd white grid and the even white grid, respectively. It is convenient to extend the even white grid by an additional white vertex dual to the exterior face of the original grid, together with edges from that new vertex to all vertices on the boundary of the even white grid (see Fig. 2). With this convention, the “extended” even white grid is simply the dual graph of the odd white grid. Note finally that the black vertices sit precisely on the edges of either of these two dual white grids.

Let us assume that we place the vacancy on a white vertex of the boundary of the grid, necessarily part of the odd white grid. Now any other vertex of the odd white grid carries a dimer [see Fig. 3(a)]. This dimer selects an edge of the odd white grid, which we decide to mark and orient from the white vertex carrying that dimer to its neighbor on the odd white grid [see Fig. 3(b) and 3(c)]. The graph made of all these marked oriented edges together with all the original vertices of the odd white grid forms a spanning tree of the odd white grid whose edges are moreover oriented toward the vacancy [see Fig. 3(d)]. To understand the absence of loops in the graph, note that a loop would enclose an interior region of the original lattice with an odd number of vertices that therefore could not be fully covered by dimers (here it is crucial that we have taken the vacancy to lie strictly on the boundary). As the graph has exactly one more vertex than edges (as the vertex carrying the vacancy does not give rise to a marked edge), it is necessarily made of a single tree spanning the whole odd white grid. The edge orientations produce the unique flow on the tree toward the vacancy (with exactly one edge exiting from all vertices but the vacancy).

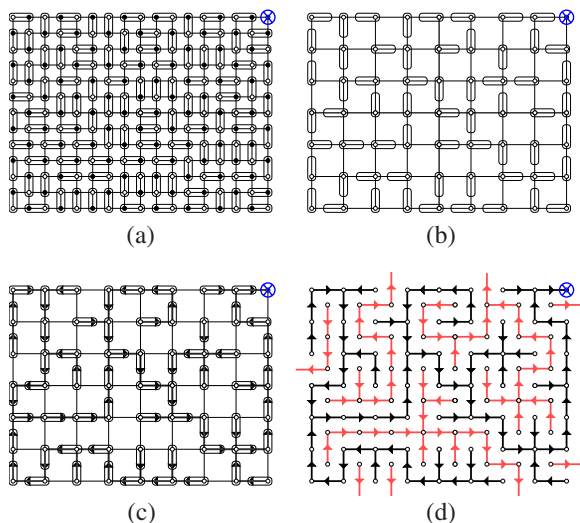


FIG. 3. (Color online) A sample dimer configuration on a 17×13 lattice (a) with a single vacancy (\otimes) in the upper right corner. In (b) we keep only those dimers that cover a vertex of the odd white grid and translate them in (c) into oriented edges of that grid, resulting in a spanning tree configuration whose edges are oriented toward the upper right corner. In (d), we also show the dual tree [red (light-gray)] which spans the extended even white grid and is oriented to the exterior face. The configuration (a) is recovered by replacing every oriented edge of (d) by a dimer on its first half.

In particular, if we fix the position of the vacancy, say in the upper right corner, the above construction provides a bijection between fully packed dimer configurations of a $(2L + 1) \times (2M + 1)$ grid with one vacancy in the corner and spanning trees of the associated $(L + 1) \times (M + 1)$ odd white grid. To go from the spanning tree configuration back to the original dimer configuration, we first orient each edge of the tree so as to reproduce the unique flow toward the upper right corner and replace each edge of the tree by a dimer on the first half of the edge. We then consider the “dual tree” of the spanning tree, made of those edges of the extended even white grid that do not cross the edges of the spanning tree. This dual graph is itself a tree spanning the extended even white grid which we orient toward the exterior vertex [see Fig. 3(d)]. We finally repeat the above construction and replace each oriented edge of the dual tree by a dimer on the first half of the edge.

Clearly, we have a similar bijection if we place the vacancy at some arbitrary but fixed white vertex on the boundary of the grid. This simply amounts to consider spanning trees with another orientation of the edges, now pointing toward the new position of the vacancy on the boundary. If we leave the position of the vacancy free along the boundary, we clearly get a $2(L + M)$ to 1 mapping instead.

Let us now consider the motion of the vacancy generated by sliding of dimers. In the tree formulation, as illustrated in Fig. 4, performing an elementary slide corresponds to picking an edge adjacent to the vacancy (and necessarily pointing to it) and reversing its orientation so that the flow now points to a new vertex. We can then repeat the process, which allows the vacancy to reach any vertex on the spanning tree, hence any vertex of the odd white grid. In the tree formula-

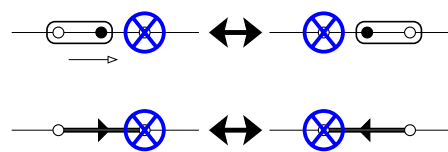


FIG. 4. (Color online) The elementary motion of the vacancy resulting from the sliding of a dimer (top). In the tree formulation, this amounts to reversing the orientation of the corresponding edge on the (oriented) spanning tree.

tion, the dimer configurations accessible by slidings are therefore described by the same spanning tree and differ only by the choice of the (arbitrary) vacancy site on the odd white grid toward which we orient all the edges of this tree. Each orientation may then be mapped into dimers as above. Note that the dimers corresponding to edges of the dual tree cannot be affected by slidings and are in practice frozen. Note, finally, that the property that the vacancy can reach any site of the odd white grid holds only because the vacancy was on the boundary in the first place. As shall see just below, this property is not true in general for vacancies that lie inside the grid. To conclude, the motion of the vacancy can be analyzed as simple diffusion on a spanning tree picked uniformly at random.

B. Extension to webs

Let us now consider the more general case where the vacancy originally lies on an arbitrary vertex of the odd white grid, not necessarily on the boundary [see Fig. 5(a)]. We can repeat the above construction by marking and orienting, for each vertex of the odd white grid except the vacancy vertex, the edge that is selected by the dimer covering that vertex [see Fig. 5(b)]. As before, we consider the graph made of all these marked oriented edges together with all the original vertices of the odd white grid. As there is exactly one oriented edge exiting from each vertex but the vacancy vertex, any connected component of this graph is either a tree containing the vacancy vertex and with edges pointing to that vertex or it is made of an oriented loop with attached branches oriented toward it [see Fig. 5(c)]. In this latter case, the connected component cannot contain the vacancy vertex. Moreover, as before, any such loop encloses an odd number of vertices, so it must encircle the vacancy, which is possible only if the vacancy does not lie on the boundary. To summarize, the general structure of the graph is a tree containing the vacancy vertex (the tree may be as small as a single vertex) surrounded by a number of nested loop components (made of a loop and attached branches) so that the graph spans the entire odd white grid. We shall call such a structure a “spanning web” of the odd white grid rooted at the vacancy vertex.

Conversely, given such a graph, we note that the “dual web” made of those edges of the extended even white grid that do not cross the edges of the spanning web is itself a spanning web of the extended even white grid [see Fig. 5(d)]. It is made of a set of nested loop components, with branches, complemented by a tree rooted at the exterior vertex. The loops of the dual web and that of the original span-

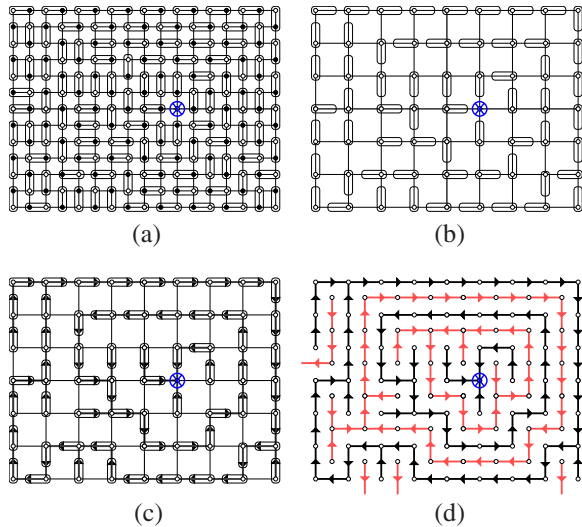


FIG. 5. (Color online) A sample dimer configuration (a) with a single vacancy (\otimes) in the bulk of the odd white grid. In (b) we show only those dimers that cover a vertex of the odd white grid. When mapping them into oriented edges of that grid, the resulting spanning web (c) consists of a tree component containing the vacancy, surrounded by a number of loop components (here 2). The edges belonging to branches of the tree component are oriented toward the vacancy while those belonging to branches of the loop components are oriented toward the loop. On each loop, all edges have the same orientation. In (d), we also show the “dual web” [red (light-gray)] which spans the extended even white grid and is made of an equal number of loop components surrounding the vacancy together with an extra tree component attached to the exterior face. The edges belonging to branches of this tree component are oriented toward the exterior face while those belonging to branches of the loop components are oriented toward the loop. Again, all edges have the same orientation on each loop. The configuration (a) is recovered by replacing every oriented edge of (d) by a dimer on its first half.

ning web alternate and therefore match in number. We can translate the spanning web configuration into a dimer configuration by successively orienting the edges of its tree component toward one of its vertices, where we put the vacancy, the edges of each loop in the same direction, chosen arbitrarily for each loop, and finally the edges of the attached branches toward the loops. Similarly, we orient the edges of the tree component of the dual web toward the exterior vertex, those of the loops in the same direction, arbitrarily for each loop and those of the attached branches toward the loops. The dimer configuration is obtained by replacing each of these oriented edges by a dimer on the first half of the edge.

The above construction provides a bijection between dimer configurations with a vacancy at a fixed position on the odd white grid and spanning webs whose tree component contains the vacancy, together with a choice of orientation for each loop of the spanning web and each loop of the dual web. As there are two possible orientations per loop and an equal number of loops on both web configurations, we can get rid of the orientations by counting each loop of the original spanning web with a degeneracy factor 4.

Again, let us examine how the vacancy can move under the sliding of dimers. As before, an elementary slide amounts in the spanning web language to reversing the orientation of one edge pointing to the vacancy so that it points to a new vertex. Under repeated moves, the vacancy can reach every white site of the tree component of the spanning web, which therefore constitutes a complete specification of the set of sites accessible to the vacancy. Note that all the dimers corresponding to oriented edges of either the loop components of the spanning web or any component of its dual web are frozen. In particular, the vacancy cannot cross a loop of either web.

On a finite grid, we may therefore divide the configurations into two classes, depending on whether or not the vacancy can reach the boundary. If the vacancy can reach the boundary, there cannot be any loop as the loops are required to encircle the tree component of the spanning web. In this case, the spanning web reduces to a spanning tree and the vacancy can reach any vertex of the odd white grid. If the vacancy cannot reach the boundary, there must be a loop component containing all the white boundary vertices. There are in general several nested loops, the interior-most one acting as a cage for the vacancy. The motion of the vacancy may then be analyzed as simple diffusion on the tree component of the web. For a fixed initial position of the vacancy on the grid, the ratio between the number of dimer configurations for which the vacancy can reach the boundary and the total number of dimer configurations can be interpreted as a delocalization probability. This probability will be studied in detail in Sec. III A below for the case of a square grid with vacancy in the center. On an infinite grid, the vacancy is always localized to a finite tree component but we shall see that the mean size of this tree in fact diverges.

C. Determinant formulas

It is well known that the number of spanning trees on a graph with n vertices is given by any principal $(n-1) \times (n-1)$ minor of the Laplacian matrix of this graph. This is the celebrated matrix-tree theorem attributed to Kirchhoff [14]. Recall that the coefficients of the Laplacian matrix simply read

$$\Delta_{ij} = \begin{cases} d_i & \text{for } i=j, \\ -1 & \text{for } i \text{ and } j \text{ neighbors,} \\ 0 & \text{otherwise,} \end{cases} \quad (2.1)$$

where i and j are vertices of the graph and d_i is the degree of i (number of incident edges) on the graph.

Here we are interested in the case of a rectangular grid where d_i can be 2, 3, or 4 according to whether i lies at a corner, on the side or in the bulk of the grid. Computing the minor amounts to removing a given vertex i_0 , i.e. restricting the indices of the matrix to all $i \neq i_0$. Note that although i_0 is

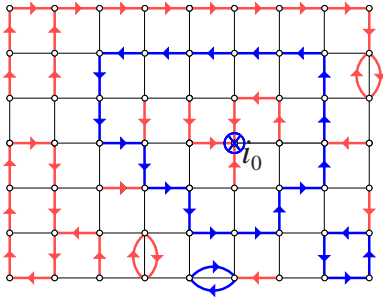


FIG. 6. (Color online) A graphical representation of a term in the expansion of the determinant in Eq. (2.2) by use of oriented “blue” and “red” edges. There is exactly one outgoing arrow from every vertex distinct from i_0 . Blue (dark) edges must form oriented cycles, each cycles receiving a weight -1 . Red (light-gray) edges may either form oriented cycles or branches oriented toward a (blue or red) cycle or toward i_0 .

removed, the degrees of its neighbors are kept unchanged. The number Z_{tree} of spanning trees therefore reads

$$Z_{\text{tree}} = \det(\Delta_{ij})_{i,j \neq i_0}. \quad (2.2)$$

Let us sketch a proof of this result, along the lines of Ref. [15], that can be easily extended to spanning webs. Writing the determinant as a sum over permutations, we see that the only permutations having a nonzero contribution are those with the following two types of cycles: (i) trivial cycles of length one (fixed points), each contributing a weight equal to the degree the associated vertex, and (ii) cycles of length larger or equal to 2 for which any two successive elements of the cycle are neighbors on the grid. The net contribution of any such nontrivial cycle to the determinant (including the signature of the permutation) is easily seen to be -1 . It is convenient to have a pictorial representation of each such permutation as follows. Any cycle of type (ii) above can be represented as a closed oriented loop on the grid by joining each vertex to its image under the permutation. The loops moreover avoid the removed vertex i_0 . Such loops are represented in blue (dark) in Fig. 6 and will be henceforth referred to as blue loops. Each blue loop contributes a factor -1 . For the trivial cycles (i), the contribution d_i of the associated vertex i is properly accounted for by considering the d_i possible choices of an edge incident to that vertex. For each choice, we mark and orient the edge away from the vertex.

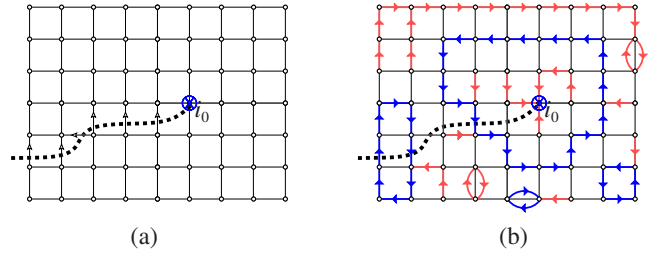


FIG. 7. (Color online) The odd white grid (a) completed with a seam from i_0 to the boundary (thick dashed line). This seam crosses a number of edges that we call seam edges and that we orient so as to point to the right when flowing on the seam from i_0 to the boundary. In the graphical expansion of the determinant (b), the seam modifies the weight of the blue (dark) edges crossing it, resulting in a new weight for blue loops. Here the blue loop that winds around i_0 passes through exactly one seam edge (with the wrong orientation), resulting in a weight factor $-1/a$ instead of -1 in the absence of a seam. On the contrary, the lower-left blue loop that does not wind around i_0 passes exactly twice through seam edges, with canceling orientations so that its weight is unchanged.

Such oriented edges are represented in red (light gray) in Fig. 6 and will be referred to as red edges. Any permutation is thus represented by a number of configurations (corresponding to the different choices of red edges for trivial cycles) made of blue loops and red edges with the only constraint that there is exactly one outgoing (blue or red) edge from each vertex of the grid but the removed vertex i_0 . Each configuration is now weighted by a factor 1 per red edge and -1 per blue loop. Now clearly, any configuration in which the red edges form a loop is canceled exactly by a similar configuration where all the edges of this loop are blue. The only configurations that remain therefore consist of red edges forming a spanning tree, necessarily oriented toward the removed vertex i_0 . This completes the proof. From the determinant formula in Eq. (2.2), one can easily derive a closed formula for Z_{tree} as a product over eigenvalues of Δ [16].

The expression (2.2) is easily modified to obtain the number $Z_{\text{web}}(i_0)$ of spanning webs on a rectangular grid rooted at some fixed vertex i_0 . We simply construct an oriented seam from i_0 to the exterior face that crosses edges only (see Fig. 7). Each crossed edge, which we denote a seam edge, can be oriented so as to point right when flowing along the seam. We may then modify the Laplacian matrix into a matrix $\Delta(a)$ defined as

$$\Delta(a)_{ij} = \begin{cases} d_i & \text{for } i = j, \\ -1 & \text{for } i, j \text{ neighbors not separated by a seam edge,} \\ a & \text{for } i, j \text{ neighbors separated by a seam edge oriented from } i \text{ to } j, \\ \frac{1}{a} & \text{for } i, j \text{ neighbors separated by a seam edge oriented from } j \text{ to } i, \\ 0 & \text{otherwise.} \end{cases} \quad (2.3)$$

For any choice of the seam, the quantity

$$Z(y; i_0) \equiv \det[\Delta(a)_{ij}]_{i,j \neq i_0} \quad (2.4)$$

then counts the number of spanning webs with root i_0 and with a weight

$$y = 2 - a - \frac{1}{a} \quad (2.5)$$

per loop. In particular, we recover $Z_{\text{tree}} = Z(0; i_0)$ for $a=1$ while for spanning webs, the desired weight 4 per loop is obtained by choosing $a=-1$, i.e.,

$$Z_{\text{web}}(i_0) = Z(4; i_0) = \det[\Delta(-1)_{ij}]_{i,j \neq i_0}. \quad (2.6)$$

To obtain this result, we simply use for the determinant the same representation as above in terms of blue loops and red edges. Defining the algebraic number of seam crossings as the number of passages across seam edges in the correct orientation minus that in the wrong orientation, this number is zero for a loop that does not encircle i_0 , +1 for a loop that encircles i_0 clockwise, and -1 for a loop that encircles i_0 counterclockwise. The blue loops that wind around the vertex i_0 now get a modified weight $-a$ or $-1/a$ according to whether they are oriented clockwise or counterclockwise. As the weight of red edges is unaffected, any clockwise (counterclockwise) red loop encircling the vertex i_0 combined with the same configuration with a blue loop instead gives rise to a weight $1-a$ (respectively $1-1/a$). Summing over both orientation results in the weight y above.

III. FINITE SIZE ANALYSIS

A. Determinant calculations and asymptotic estimates

In this section, we shall restrict our analysis to the case of dimers on a square grid with the vacancy in the center. We shall consider only squares of size $(4L+1) \times (4L+1)$ so that the center vertex i_0 lies on the odd white grid, of size $(2L+1) \times (2L+1)$. With this geometry, we can rely on the four-fold rotational symmetry of the problem to perform a block diagonalization of $\Delta(a)$ which translates into the factorization

$$Z(y; i_0) = P_L(\alpha)P_L(-\alpha)P_L(i\alpha)P_L(-i\alpha), \quad (3.1)$$

where $\alpha^4 = a$ with a as in Eq. (2.5), namely,

$$y = 2 - \alpha^4 - \frac{1}{\alpha^4}. \quad (3.2)$$

Here $P_L(\alpha)$ is the determinant of a square matrix $\bar{\Delta}(\alpha)$ of size $L(L+1)$ [compared to $4L(L+1)$ for $\Delta(a)$] corresponding to a modified Laplacian on a quarter grid. More precisely, we consider the graph of Fig. 8 obtained by keeping only one quadrant of the original odd white grid and completing it by adding L oriented “winding edges” joining the vertices of two consecutive sides of the quadrant as shown. The matrix $\bar{\Delta}(\alpha)$ has diagonal elements $\bar{\Delta}(\alpha)_{ii} = d_i$, where d_i is the degree of site i on the graph of Fig. 8 completed by the vertex i_0 as shown, which is also the degree of the corresponding vertex

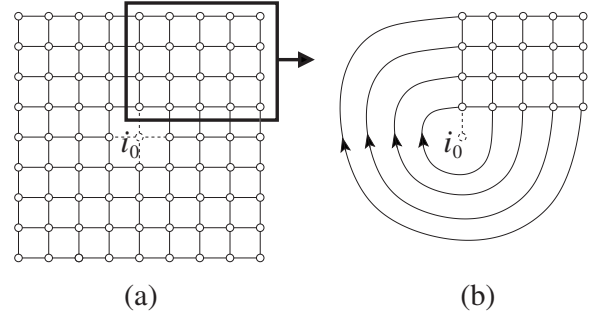


FIG. 8. The reduction of the odd white grid (a) to one of its quadrants (b) completed by oriented winding edges.

on the original odd white grid. The off-diagonal elements $\bar{\Delta}(\alpha)_{ij}$ are given by the sum over all edges connecting i and j of a contribution equal to -1 for regular (nonwinding) edges, $-\alpha$ (respectively $-1/\alpha$) for winding edges oriented from i to j (from j to i).

It is interesting to note that $P_L(\alpha)$ can be interpreted as the number of spanning web configurations rooted at the center of the square grid of size $(2L+1) \times (2L+1)$ and which are symmetric under $\pi/2$ rotations around the vacancy vertex. For any such symmetric spanning web, the loops now come with a weight $y = 2 - \alpha - 1/\alpha$. In particular, for $\alpha = -1$, $P_L(-1)$ counts the number of fourfold symmetric dimer configurations on the square grid of size $(4L+1) \times (4L+1)$.

Using MATHEMATICA, we have computed $P_L(\alpha)$ exactly up to $L=60$, corresponding to dimers on a 241×241 grid. For $L=1, 2, 3$, we have

$$\begin{aligned} P_1(\alpha) &= 4 - \left(\alpha + \frac{1}{\alpha} \right), \\ P_2(\alpha) &= 178 - 60 \left(\alpha + \frac{1}{\alpha} \right) + \left(\alpha^2 + \frac{1}{\alpha^2} \right), \\ P_3(\alpha) &= 82128 - 31667 \left(\alpha + \frac{1}{\alpha} \right) + 1160 \left(\alpha^2 + \frac{1}{\alpha^2} \right) \\ &\quad - \left(\alpha^3 + \frac{1}{\alpha^3} \right). \end{aligned} \quad (3.3)$$

More generally, $P_L(\alpha)$ is a Laurent polynomial of α of the form

$$P_L(\alpha) = \sum_{i=-L}^L \pi_{L,i} (-\alpha)^i, \quad (3.4)$$

where the $\pi_{L,i}$ are positive integers and satisfy $\pi_{L,-i} = \pi_{L,i}$. Their numerical values for $L=10, 20, 30, 40, 50$, and 60 are displayed in Fig. 9.

From our data, we first conjecture the amusing fact that $P_L(i)$ counts the number of fully packed dimer configurations on a cylinder of height $2L$ and circumference $2L+1$. More relevant to our study, we expect a large L behavior

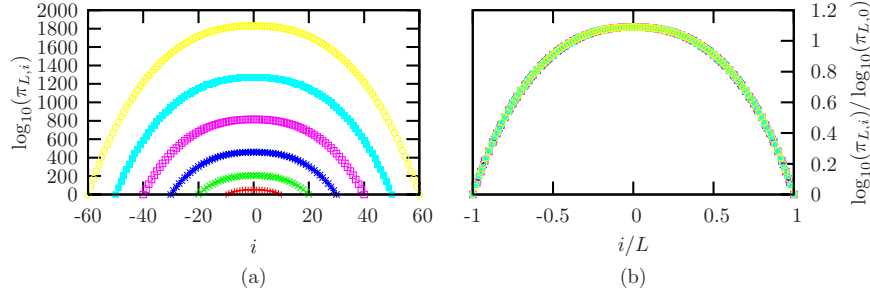


FIG. 9. (Color online) The numerical value (a) of $\log_{10}(\pi_{L,i})$ versus i for $L=10, 20, 30, 40, 50,$ and 60 , from bottom to top. All the data fall on the same scaling curve (b) upon using reduced variables i/L and $\log_{10}(\pi_{L,i})/\log_{10}(\pi_{L,0})$.

$$P_L(\alpha) \sim \tilde{c}(\alpha) \frac{\mu^{L(L+1)} \lambda^L}{L^{\tilde{\gamma}(\alpha)}}, \quad (3.5)$$

where the area entropy factor μ and the boundary entropy factor λ are independent of α while the prefactor c and the exponent $\tilde{\gamma}$ depend on α . The values of μ and λ are known to be [16]

$$\begin{aligned} \mu &= \exp\left(\frac{1}{4\pi^2} \int_0^{2\pi} dk \int_0^{2\pi} dl \ln(4 - 2\cos k - 2\cos l)\right) \\ &= \exp\left(\frac{4G}{\pi}\right) = 3.209912300728158\dots, \end{aligned}$$

$$\lambda = \sqrt{2} - 1, \quad (3.6)$$

where $G = \sum_{i=0}^{\infty} (-1)^i / (2i+1)^2$ is Catalan's constant. We have checked the consistency of our exact finite size data with these values. For instance, the value of μ can be estimated by considering the ratio $A_L(\alpha) = P_{L+2}(\alpha)P_L(\alpha) / [P_{L+1}(\alpha)]^2$, which converges to μ^2 at large L , and applying to A_L standard convergence acceleration techniques. In this paper, we found it convenient to use a simple linear convergence algorithm which consists, for any sequence U_L tending at large L to U_{∞} , in building new sequences $U_L^{(k)} = \Delta^{(k)}[L^k U_L / k!]$ for increasing integers k , where $\Delta^{(k)}$ denotes the k th iteration of the finite difference operator $\Delta f(L) \equiv f(L+1) - f(L)$. The sequence $U_L^{(k)}$ is expected to tend faster to U_{∞} for larger k as long as k is kept reasonably small (in practice we used mostly $k=4$ and went as far as $k=11$ for the jamming prob-

ability of Sec. III B below). For instance, if U_L has a Taylor expansion in $1/L$, then the Taylor expansion of $U_L^{(k)}$ has its first k correction terms vanishing.

The estimates for μ when $\alpha=+1$ and $\alpha=-1$ are plotted in Fig. 10 as a function of L . We obtain the value $\mu = 3.2099123(1)$, fully consistent with the exact analytic expression above.

More interesting is the value of the exponent $\tilde{\gamma}$. Here we shall be interested only in real values of y in the range $[0, 4]$. This corresponds to taking complex values of α on the unit circle. The value of $\tilde{\gamma}$ can be estimated from the quantity $B_L = -(L^3/2) \ln(P_{L+3}(\alpha)[P_{L+1}(\alpha)]^3 / P_L(\alpha)[P_{L+2}(\alpha)]^3)$, which converges to $\tilde{\gamma}(\alpha)$ at large L . Again the results are improved by use of our convergence acceleration algorithm.

Figure 11 displays the estimated values of $\tilde{\gamma}$ as a function of L for the various values of α corresponding to $y=0$ ($\alpha^4=1$) and $y=4$ ($\alpha^4=-1$). We obtain the asymptotic estimates

$$\tilde{\gamma}(1) = 0.749999(1),$$

$$\tilde{\gamma}(-1) = -0.249999(1),$$

$$\tilde{\gamma}(i) = \tilde{\gamma}(-i) = 0.000000(1) \quad (3.7)$$

for the four roots of $\alpha^4=1$ and

$$\tilde{\gamma}[\exp(i\pi/4)] = \tilde{\gamma}[\exp(-i\pi/4)] = 0.3125002(2),$$

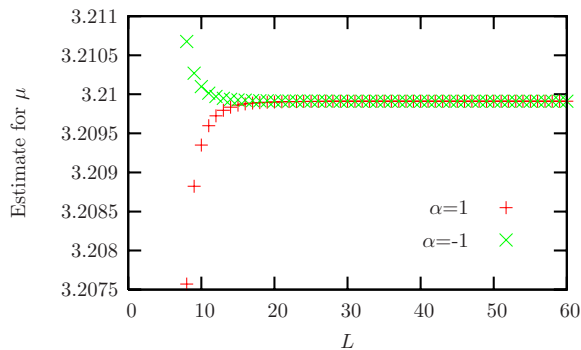


FIG. 10. (Color online) Estimate for the area entropy μ at $\alpha=\pm 1$ from the data of $P_L(\alpha)$ for L up to 60.

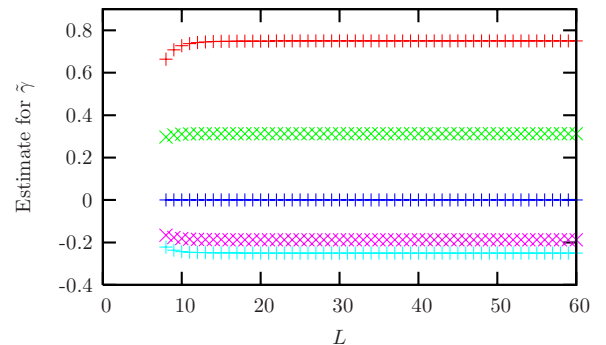


FIG. 11. (Color online) Estimates of the exponent $\tilde{\gamma}(\alpha)$ for, from top to bottom, $\alpha=1$, $\alpha=\exp(\pm i\pi/4)$, $\alpha=\pm i$, $\alpha=\exp(\pm 3i\pi/4)$, and $\alpha=-1$, as obtained from the data of $P_L(\alpha)$ for L up to 60.

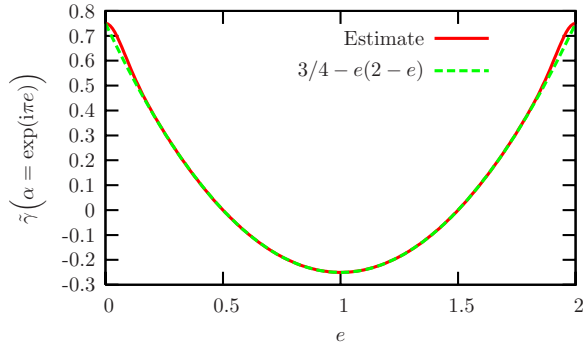


FIG. 12. (Color online) Estimated value of $\tilde{\gamma}(\alpha)$ for $\alpha = \exp(i\pi e)$ with $0 \leq e \leq 2$, as obtained from the data of consecutive values of $P_L(\alpha)$ for L near 60 (red solid line). The green (dashed) line indicates the conjectured exact result $\tilde{\gamma}(\alpha) = 3/4 - e(2-e)$.

$$\tilde{\gamma}[\exp(3i\pi/4)] = \tilde{\gamma}[\exp(-3i\pi/4)] = -0.187499(1) \quad (3.8)$$

for the four roots of $\alpha^4 = -1$. From these estimates, we conjecture the exact values

$$\tilde{\gamma}(1) = 3/4,$$

$$\tilde{\gamma}(-1) = -1/4,$$

$$\tilde{\gamma}(i) = \tilde{\gamma}(-i) = 0,$$

$$\tilde{\gamma}[\exp(i\pi/4)] = \tilde{\gamma}[\exp(-i\pi/4)] = 5/16,$$

$$\tilde{\gamma}[\exp(3i\pi/4)] = \tilde{\gamma}[\exp(-3i\pi/4)] = -3/16. \quad (3.9)$$

More generally, Fig. 12 displays the estimate of $\tilde{\gamma}(\alpha)$ for all values of α on the unit circle. These data are fully consistent with the following analytic expression for $\tilde{\gamma}$:

$$\tilde{\gamma}(\alpha) = \frac{3}{4} - e(2-e), \quad \alpha = \exp(i\pi e), \quad 0 \leq e \leq 2. \quad (3.10)$$

This form for the exponent, quadratic in the phase e , is frequently encountered in models with statistical weights associated to loops and will be assumed exact in all subsequent analysis.

From Eq. (3.1), we immediately deduce from our data the exact generating function $Z_L(y) \equiv Z(y; i_0)$ for a $(2L+1) \times (2L+1)$ odd white grid with i_0 in the center for L up to 60. For instance, we get

$$Z_1(y) = 192 + y,$$

$$Z_2(y) = 557568000 + 10474560y + y^2,$$

$$Z_3(y) = 19872369301840986112 + 647704492383277056y + 1642581444224y^2 + y^3. \quad (3.11)$$

Note that $Z_{60}(0)$ and $Z_{60}(4)$ are 7323 digit numbers. From

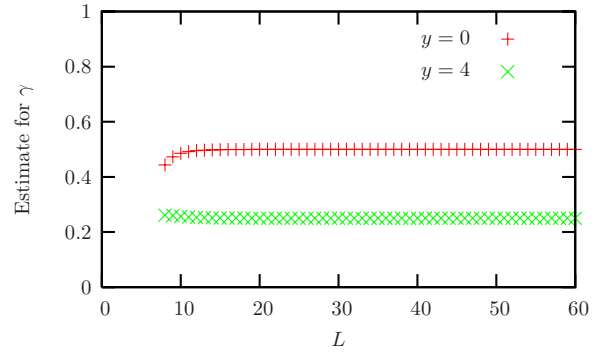


FIG. 13. (Color online) A direct estimate of the exponents $\gamma(0)$ and $\gamma(4)$ obtained from the data of $Z_L(0)$ and $Z_L(4)$ for L up to 60.

Eqs. (3.1) and (3.5), we have the following large L behavior for $Z(y; i_0)$:

$$Z(y; i_0) \sim c(y) \frac{\mu^{(2L+1)^2} \lambda^{4L}}{L^{\gamma(y)}}, \quad (3.12)$$

where $\gamma(y) = \tilde{\gamma}(\alpha) + \tilde{\gamma}(-\alpha) + \tilde{\gamma}(i\alpha) + \tilde{\gamma}(-i\alpha)$ with α as in Eq. (3.2) and $c(y) = \tilde{c}(\alpha)\tilde{c}(-\alpha)\tilde{c}(i\alpha)\tilde{c}(-i\alpha)/\mu$.

In particular, for $y=0$ ($\alpha^4=1$) and $y=4$ ($\alpha^4=-1$), we obtain $\gamma(0) = 3/4 - 1/4 + 0 + 0 = 1/2$ and $\gamma(4) = 5/16 + 5/16 - 3/16 - 3/16 = 1/4$, namely,

$$Z_{\text{tree}} \sim c(0) \frac{\mu^{(2L+1)^2} \lambda^{4L}}{L^{1/2}},$$

$$Z_{\text{web}}(i_0) \sim c(4) \frac{\mu^{(2L+1)^2} \lambda^{4L}}{L^{1/4}}. \quad (3.13)$$

Note that the first exponent (1/2) can be obtained directly from the asymptotics of the closed product formula for Z_{tree} [16]. As shown in Fig. 13, these values are corroborated by a direct estimate of γ from the exact values of $Z_L(0)$ and $Z_L(4)$ for L up to 60. We indeed estimate $\gamma(0) = 0.499999(1)$ and $\gamma(4) = 0.250001(1)$. Taking the ratio of Z_{tree} and $Z_{\text{web}}(i_0)$, we deduce that the delocalization probability \mathcal{P}_L of a vacancy at the center of a $(4L+1) \times (4L+1)$ square decays at large L as

$$\mathcal{P}_L \approx \frac{1}{L^{1/4}}, \quad (3.14)$$

with some prefactor $c(4)/c(0)$.

More generally, we immediately get from the expression (3.10) (with α restricted, without loss of generality, to $0 \leq e \leq 1/2$):

$$\gamma(y) = u^2 + \frac{1}{4}, \quad y = [2 \cos(\pi u)]^2, \quad -\frac{1}{2} \leq u \leq \frac{1}{2}, \quad (3.15)$$

where we have set $u = 1/2 - 2e$. This expression can be alternatively obtained from a heuristic argument based on an effective Coulomb gas description of the model. This argument is presented in Appendix A.

The degree of localization of the vacancy is also measured by the number \mathcal{L} of loops of the spanning web that

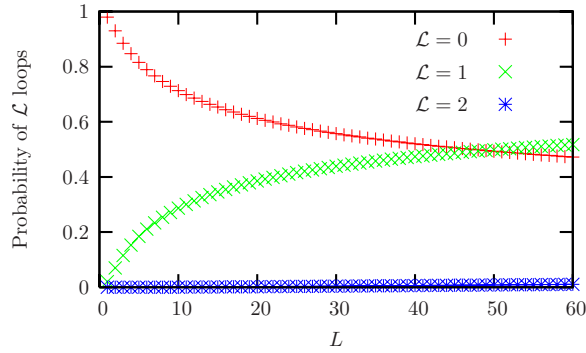


FIG. 14. (Color online) The exact probabilities for having \mathcal{L} loops in a spanning web with $y=4$ for an odd white grid of size $(2L+1) \times (2L+1)$ with the vacancy in the center. We represent only the cases of $\mathcal{L}=0,1,2$ as the other probabilities are negligible.

surround it. The average of \mathcal{L} over all spanning webs reads

$$\langle \mathcal{L} \rangle = y \frac{d}{dy} \ln Z(y; i_0). \quad (3.16)$$

At large L , we find from the asymptotic behavior (3.12) that

$$\langle \mathcal{L} \rangle \sim -y \frac{d}{dy} \gamma(y) \ln L = \frac{u}{\pi \tan(\pi u)} \ln L, \quad (3.17)$$

where we have used the explicit form (3.15) of $\gamma(y)$ with $y = [2 \cos(\pi u)]^2$. For instance, when $y=4$ (i.e., $u \rightarrow 0$), we find that the average over all possible dimer configurations of the number of loops around the vacancy scales as

$$\langle \mathcal{L} \rangle \sim \frac{1}{\pi^2} \ln L \quad (3.18)$$

at large L .

From the exact values of $Z_L(y)$, we also have access to the exact probability for spanning webs to have \mathcal{L} loops on a finite square grid with the vacancy in the center. Figure 14 displays these probabilities in the case $y=4$ for $\mathcal{L}=0$ (which is nothing but \mathcal{P}_L) and $\mathcal{L}=1,2$, with L up to 60. Note that for this range of grid sizes, the probability that $\mathcal{L} \geq 3$ is negligible (less than 10^{-5}). All these probabilities are expected to eventually decay as $L^{-1/4}$ at large L .

B. Asymptotic size distribution

We have established so far that, for a finite grid, the delocalization probability \mathcal{P}_L decreases with the system size L as a power law with exponent $1/4$. Let us now see how to extract from this result the value of two other exponents which characterize the possible motion of a single vacancy in a sea of dimers on an infinite grid. A first exponent δ characterizes the size distribution of sites accessible to a vacancy. More precisely, let us consider again a grid of size $(4L+1) \times (4L+1)$ covered by dimers with a vacancy at the center and consider the probability $p_L(s)$ that the tree component of the associated spanning web has s vertices. We expect this probability to tend at large L to some limiting law $p(s) = \lim_{L \rightarrow \infty} p_L(s)$, with a finite value for all positive integers s .

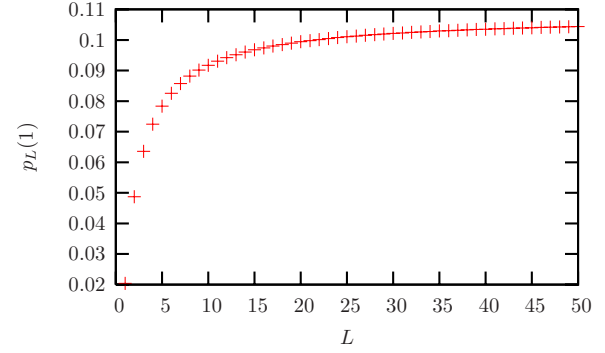


FIG. 15. (Color online) The probability $p_L(1)$ that the vacancy at the center of a $(4L+1) \times (4L+1)$ grid is strictly jammed.

This asymptotic distribution should be universal in the sense that it should not depend on the precise initial position of the vacancy in the bulk or on the imposed boundary conditions.

Of particular interest is the value of $p(1)$ which measures the probability that the vacancy is fully jammed. This value is easily estimated from the exact values of $p_L(1)$ at finite L . For $s=1$, the tree component of the spanning web is reduced to the single vertex i_0 . In the determinant formulation of Sec. II C, this simply means that no red edge points toward i_0 . Imposing $s=1$ therefore amounts to changing $d_i \rightarrow d_i - 1$ in Eq. (2.3) for the diagonal terms associated with the four neighbors of i_0 on the grid. Again we can rely on the fourfold symmetry to reduce by four the size of the matrix involved. We have computed $p_L(1)$ for L up to 50, as plotted in Fig. 15. By applying our convergence algorithm, we estimate $p(1) = 0.10786437626904951198(1)$ from which we conjecture the exact value

$$p(1) = \frac{57}{4} - 10\sqrt{2}. \quad (3.19)$$

This value was identified thanks to Plouffe's inverter [17] applied on the first 10 digits of $1/\sqrt{p(1)}$. We then verified that it indeed reproduces all 20 digits of $p(1)$ above. It would be nice to have an analytic proof of this result.

We have also computed $p_L(2)$ exactly for L up to 34, from which we estimate $p(2) = 0.055905353801942(1)$. We have not been able to guess an exact expression for $p(2)$.

At large s , the distribution $p(s)$ should behave as

$$p(s) \simeq s^{-\delta} \quad (3.20)$$

with an exponent δ that we shall now compute. First, since the delocalization probability \mathcal{P}_L tends to 0 at large L , it follows that the vacancy in an infinite system is always localized. This implies that the distribution $p(s)$ is normalized to 1, namely, $\sum_{s=1}^{\infty} p(s) = 1$.

To evaluate δ , we consider the probability $1 - \mathcal{P}_L$ that the vacancy in a finite grid is localized, i.e., cannot reach the boundary of the grid. At large L , we can indeed estimate this probability as the probability that s remains less than a maximal size of order $4L^2$, namely,

$$\begin{aligned}
 1 - \mathcal{P}_L &\sim \sum_{s=1}^{4L^2} p(s) \\
 &= 1 - \sum_{s=4L^2+1}^{\infty} p(s) \\
 &\sim 1 - \int_{4L^2}^{\infty} p(s) ds \sim 1 - \text{const } L^{2(1-\delta)}. \quad (3.21)
 \end{aligned}$$

Comparing with Eq. (3.14), one finds

$$2(1 - \delta) = -\frac{1}{4}, \quad (3.22)$$

from which we deduce

$$\delta = \frac{9}{8}. \quad (3.23)$$

Despite the fact that the vacancy is localized on a finite tree, the result that $\delta < 2$ implies that the mean size $\langle s \rangle$ of this tree nevertheless diverges. For some observables, the vacancy behaves on average as if it were delocalized. In this sense, our model possesses a rather unusual property which we may call weak localization.

C. Diffusion exponent

As an illustration of this unusual property, let us now discuss the dynamics of diffusion of a single vacancy in a dense sea of dimers. As we discussed, the motion of the vacancy is induced by a dimer sliding axially into it, resulting in a jump of the vacancy by two lattice spacings. In the spanning web language, this simply amounts to moving the vacancy to one of its neighbors on the tree component of the spanning web. A natural choice of dynamics consists of choosing, at each time step, one of the four neighbors of the vacancy on the odd white grid at random, and moving the vacancy to that neighbor if possible, i.e., if this neighbor belongs to the tree component of the spanning web. We then define $S(t)$ as the total number of sites visited by the vacancy after t steps. Although $S(t)$ is clearly bounded by the size s of the tree component of the spanning web, we expect from our weak localization property that it can become on average arbitrarily large, with a large time behavior of the form

$$\langle \bar{S}(t) \rangle \sim kt^\eta, \quad (3.24)$$

with some constant k . Here we first average over all possible motions of the vacancy up to time t [$\bar{S}(t)$] for a fixed initial sea of dimers (with the vacancy in the center) and then average over uniformly chosen realizations of this initial dimer configuration.

It is natural to compare this diffusion to that of a particle diffusing with the same dynamical rules on a uniformly chosen infinite spanning tree. This latter diffusion is characterized by a similar exponent η_0 with

$$\langle \bar{S}(t) \rangle_0 \sim k_0 t^{\eta_0}, \quad (3.25)$$

where the average $\langle \cdots \rangle_0$ is now taken over all possible (infinite) spanning trees.

A simple scaling argument relates the exponents η and η_0 . Denoting by s the size of the tree component of the spanning web for a fixed dimer configuration, we expect that $\bar{S}(t) \sim k_0 t^{\eta_0}$ with the infinite spanning tree diffusion exponent η_0 as long as $k_0 t^{\eta_0}$ is less than s , while it saturates at $\bar{S}(t) \sim s$ for longer times. Using Eq. (3.20) for the distribution of sizes s , we can estimate

$$\langle \bar{S}(t) \rangle \sim \int_0^{k_0 t^{\eta_0}} ds s p(s) + \int_{k_0 t^{\eta_0}}^{\infty} ds k_0 t^{\eta_0} p(s) \simeq t^{\eta_0(2-\delta)}. \quad (3.26)$$

Note that it is crucial that $1 < \delta < 2$ for the two integrals to scale in the same way, determined by the t -dependent limits of the integrals. In other words, the weak localization property of our model is essential for a well defined scaling. Taking $\delta = 9/8$, we have the relation

$$\eta = \frac{7}{8} \eta_0, \quad (3.27)$$

which measures the lowering of the diffusion exponent due to weak localization.

IV. MONTE CARLO SIMULATIONS

A. Simulations of spanning webs

We have also found it revealing to perform numerical simulations of our model. As we shall see, we find very good agreement for all quantities for which we gave analytic predictions. Moreover, the simulations allow us to estimate both diffusion exponents η and η_0 independently, as well as other dynamical exponents.

To begin with, we have simulated spanning webs using a modification of the Propp-Wilson cycle-popping algorithm for finding spanning trees of an arbitrary directed graph [18]. This algorithm is presented in detail in Appendix B and works as follows: for every vertex of the odd white grid other than the vacancy vertex, we pick a possible outgoing arrow at random. If the resulting graph contains one or more cycles, we choose a cycle and ‘‘pop’’ it by picking a new random outgoing arrow for every vertex on the cycle. We then keep popping cycles until no cycle is left, resulting in a spanning tree. Propp and Wilson were able to show that this process terminates with probability one, and that the final result is independent of the order in which cycles are popped and produces trees uniformly distributed in the space of spanning trees. To generate spanning webs, we simply modified this algorithm by not popping cycles that encircle the vacancy. The proofs in Ref. [18] generalize straightforwardly to show that the modified algorithm results in web configurations uniform in the space of spanning webs. More precisely, this algorithm produces spanning webs with oriented loops, hence corresponding to a weight $y=2$ per loop. It is

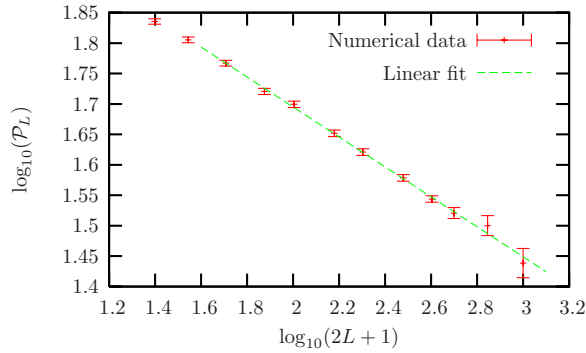


FIG. 16. (Color online) Fraction of delocalized configurations \mathcal{P}_L as a function of the system size.

then straightforward to correct for this weight so as to get an arbitrary value of y .

As a preliminary check, we have confirmed that for a number of system sizes less than 50, the algorithm produces probabilities for the number of loops (in practice 0, 1, or 2) in good agreement with the exact probabilities obtained for $y=2$ by the methods of Sec. III A.

We generated $y=2$ spanning webs on odd white grids of size $(2L+1) \times (2L+1)$ with the vacancy at the center [these correspond to dimer grids of sizes $(4L+1) \times (4L+1)$]. Our system sizes were $2L+1=25, 35, 51, 75, 101, 151, 201, 301, 401, 501, 701$, and 1001. The number of spanning webs generated was 25 000 for all system sizes $2L+1 \leq 301$, 30 000 for $2L+1=401$, 10 000 for $2L+1=501$, 3000 for $2L+1=701$, and 1500 for $2L+1=1101$. The results were then transformed into probabilities for $y=4$ spanning webs (dimer packings) by weighting configurations with \mathcal{L} loops by an extra factor $2^{\mathcal{L}}$.

The delocalization probability is measured by the fraction of spanning trees among spanning webs. This fraction is shown in Fig. 16 as a function of the system size and is well fit by a power law. Dropping the two smallest system sizes ($2L+1=25$ and $2L+1=35$), which are still consistent with a power law fit but are too small to be safely in the large system limit, we get a delocalization exponent 0.246 ± 0.006 , in agreement with the value $1/4$ predicted in Eq. (3.14).

As for the distribution $p(s)$, we first checked that the probability $p_L(1)$ of a fully jammed state is in good agreement with both the exact value that we obtained for small system sizes ($L \leq 50$) and with the asymptotic prediction of Eq. (3.19) for $p(1)$ (see Fig. 17). The distribution $p_L(s)$ for $L=200$ is shown in Fig. 18. At this stage, it is important to analyze the effect of the boundary in a finite size grid, which can be described as follows: whenever the tree component of the spanning web touches the boundary, it must span the whole grid, hence has size $(2L+1)^2$. For $s \leq L$, the tree component cannot reach the boundary so we expect $p_L(s)$ to be an accurate estimate of the asymptotic $p(s)$. For $L < s \leq (2L-1)^2$, $p_L(s)$ should become significantly lower than $p(s)$ as s increases since configurations that contribute to $p_L(s)$ are required to avoid the boundary, a constraint that does not exist in the asymptotic limit. Finally, the only possible value with $s > (2L-1)^2$ is $s=(2L+1)^2$ and corresponds to delocalized configurations, with a value $p_L[(2L+1)^2]=\mathcal{P}_L$ that is not di-

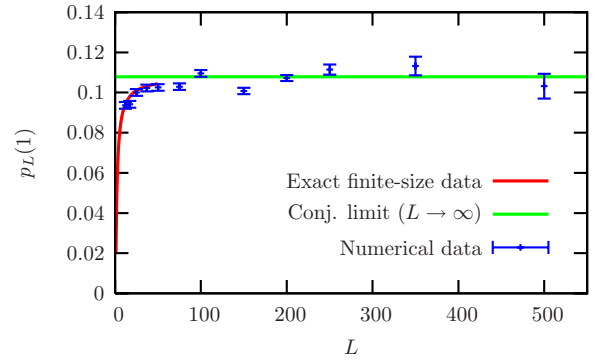


FIG. 17. (Color online) Comparison between the exact finite size values of $p_L(1)$, together with its conjectured exact asymptotic value, and the numerical probability of strict jamming.

rectly relevant to estimating $p[(2L+1)^2]$. This value is not shown in Fig. 18. By eye, the distribution appears to be a power law over almost four decades. Upon fitting the data however, a small but significant curvature appears for tree sizes greater than $10^{2.5}$, as expected from the above argument. To obtain the exponent, we thus fit only for tree sizes less than 200 (trees that cannot reach the boundary), which gives a power law exponent $\delta=1.122 \pm 0.008$, in good agreement with the prediction $\delta=9/8=1.125$ of Eq. (3.23). It is surprising that the power law fit of the data extends all the way down to $s=1$. In other words, the data are well approximated by a (normalized) pure power law distribution $s^{-9/8}/\zeta(9/8)$. For $s=1$, it gives a value $1/\zeta(9/8)=0.116 \dots$, to be compared with the exact value $0.108 \dots$ of Eq. (3.19).

As we mentioned above, we expect that the asymptotic distribution $p(s)$ should not depend on the finite size boundary conditions from which it is determined. In this vein, we have also generated dimer packings with periodic boundary conditions, for grids of odd linear size with a single vacancy. Note that the spanning web construction, central to this paper, no longer applies as, in particular, we have lost the global notion of distinct odd and even white grids in this case,

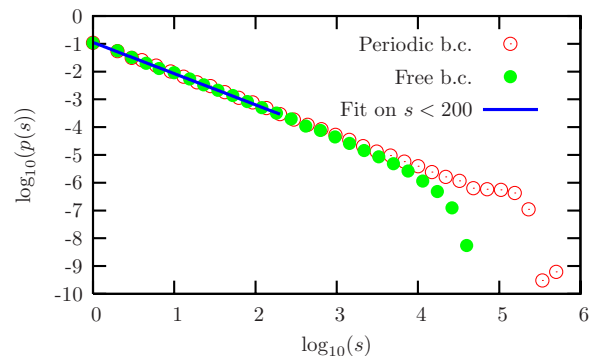


FIG. 18. (Color online) Distribution $p(s)$ for the size s of the tree component as measured from spanning web simulations with free boundary conditions (green filled circles) on a 401×401 odd white grid (corresponding to a 801×801 dimer grid) with the vacancy at the center, and directly from dimer simulations with periodic boundary conditions (red open circles) on a 1101×1101 dimer grid. The fit (blue line) is for free boundary conditions and tree sizes less than 200.

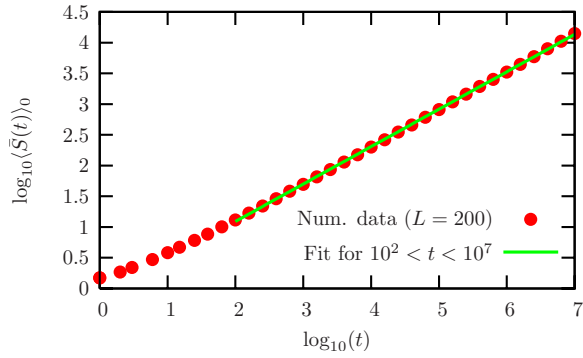


FIG. 19. (Color online) Number of distinct sites visited by a diffusing vacancy on a 401×401 uniform spanning tree as a function of time.

or even the global notion of bicolorability. Still, these notions are preserved locally and for localized configurations with small enough s , the set of accessible sites again forms a tree whose statistics we can analyze along the same lines as for free boundary conditions.

One advantage of periodic boundary conditions is that one can quickly generate many configurations, directly in the dimer setting, with the so-called “pivot algorithm” [19,20]. Since there is no longer the constraint for localized configurations of avoiding the boundary, periodic boundary conditions have the further advantage of reaching larger values of s at fixed L , leading to smaller finite size effects. For a linear size of 1101 (corresponding to $L=275$ in the spanning web language), the resulting tree size distribution is well fit by a power law over a larger range (tree sizes $1 \leq s \leq 10^{4.5}$) than for spanning webs, with an exponent $\delta=1.121 \pm 0.003$, in good agreement with Eq. (3.23). Looking at system sizes ranging from 101 to 1101, in steps of 100, we find that the fraction of delocalized configurations (now defined as configurations in which the vacancy can reach any vertex) has a power law exponent of 0.260 ± 0.005 , again in agreement with Eq. (3.14).

B. Vacancy diffusion

Let us now come to the prediction (3.27) relating the diffusion exponent η for the growth with time of the number of sites visited by a diffusing vacancy to the corresponding exponent η_0 for diffusion on an infinite spanning tree. To our knowledge, none of these exponents is known exactly and we therefore simulated both diffusion processes.

For diffusion on uniform spanning trees, the simulations were done for free boundary conditions on a 401×401 grid, with the diffusing vacancy initially at the center of the lattice. At each time step, the vacancy chooses one of the four compass directions at random and attempts a move in that direction. If there is a tree edge in that direction the move is carried out and otherwise, the vacancy stays at the same position. This slightly unusual random walk rule is chosen to mimic the standard Monte Carlo dynamics for the underlying dimers, where each time-step consists of an attempted dimer move. This means that a vacancy that has more possible moves should on average wait less time before moving.

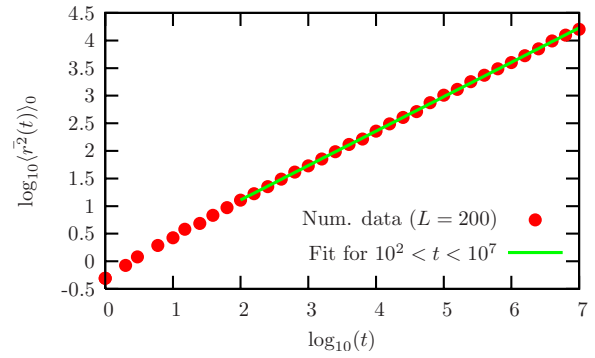


FIG. 20. (Color online) Squared displacement of a diffusing vacancy on a 401×401 uniform spanning tree as a function of time.

An ensemble of 1000 spanning trees was generated and, for each tree, the vacancy underwent 10^7 time steps. The resulting graphs for the number of sites visited as a function of time, and the squared displacement as a function of time, are shown in Figs. 19 and 20. There is a relatively large curvature at smaller times ($t < 100$), so such times are excluded from the fit. Both graphs show good power law behavior by eye over the last five decades of time. Closer inspection shows that both graphs do have a small but significant curvature, which we use to estimate the error bars of the slope (the statistical errors are negligible).

From Fig. 19, we obtain $\eta_0=0.61 \pm 0.02$, while from Fig. 20, we get $\theta_0=0.62 \pm 0.02$, where we have defined the exponent θ_0 through

$$\langle \overline{r^2}(t) \rangle_0 \propto t^{\theta_0}, \quad (4.1)$$

where $r(t)$ is the Euclidean distance of the vacancy to the center of the grid at time t . These estimates are consistent with the two exponents being identical.

We then simulated the diffusion of a vacancy on spanning webs. The spanning webs were generated with the algorithm described in Sec. IV A. An ensemble of 10 000 spanning webs was generated, each of the same size 401×401 as for the spanning trees above. For each web, the vacancy moved for the same total time and with the same dynamics as before.

Figures 21 and 22 show the number of sites visited and

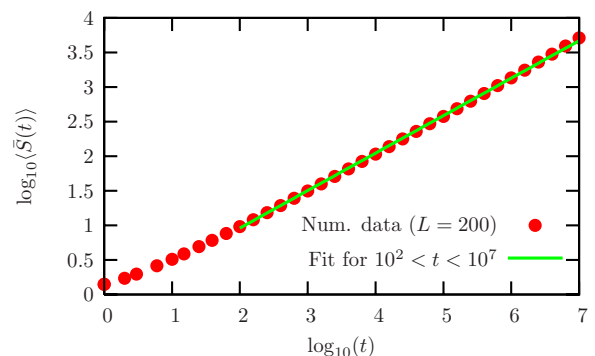


FIG. 21. (Color online) Number of distinct sites visited by a diffusing vacancy on a 401×401 uniform spanning web as a function of time.

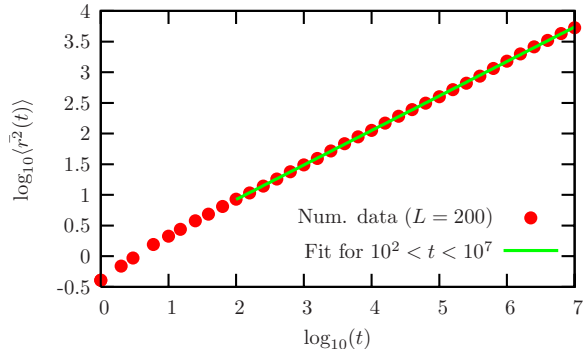


FIG. 22. (Color online) Squared displacement of a diffusing vacancy on a 401×401 uniform spanning web as a function of time.

the squared displacement in the case of spanning webs. Again, we fit only for times $t > 100$, and use the curvature to estimate the error bars. Good power law behaviors are again seen over five decades. We obtain $\eta = 0.54 \pm 0.03$ and $\theta = 0.56 \pm 0.01$ (with θ defined as θ_0 but for spanning webs). Again, these estimates are consistent with the two exponents being identical. Finally, we estimate the ratio $\eta/\eta_0 = 0.89 \pm 0.06$, in agreement with the prediction $7/8 = 0.875$ of Eq. (3.27).

V. DISCUSSION

In this paper, we have analyzed the possible motion of an isolated vacancy in an otherwise fully packed dimer model on the square lattice. We find that the vacancy exhibits weak localization: the size of its accessible domain scales as a power law with diverging average size. Exact finite size enumerations allowed us to identify several exponents as well as determine the probability for strict jamming. Some of these results are still awaiting exact and/or rigorous proofs. We also gave a universal relation between the exponents η and η_0 for the diffusion on spanning webs (vacancy diffusion) and that on spanning trees. We have no prediction for their individual values but from the numerical data, η_0 is consistent with a simple value $5/8$, which would result in a vacancy diffusion exponent η equal to $35/64$.

The emergence of spanning webs as generalizations of spanning trees is quite natural here and one might hope that they will appear in other physical and mathematical problems.

There are several directions in which the present work can be extended. Introducing multiple vacancies will lead to vacancy interactions whose treatment will almost certainly require more elaborate geometrical structures. The power of the analysis in this paper relies heavily on special features of the square lattice. Extension to other lattices will require new insight. Key among them is the triangular lattice, for which we expect vacancies to be localized, with the size distribution of accessible sites now decaying exponentially at a rate determined by the known entropy mismatch between dimer configurations and spanning tree configurations. If we assume that this size is a good measure of the extent to which a vacancy perturbs its dimer background, the localization

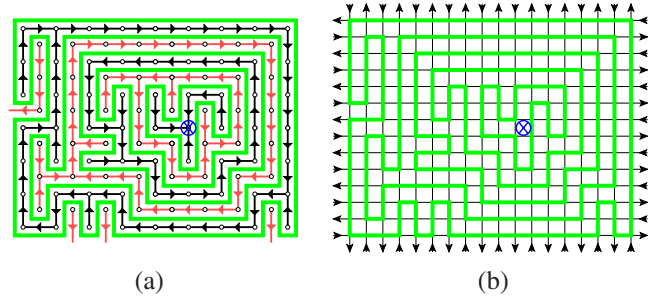


FIG. 23. (Color online) (a) The paths of the maze made of a spanning web (black) and its dual web [red (light-gray) lines with arrows] form a set of loops [thick green (light-gray) closed lines] that completely encode the (unrooted) spanning web. (b) The loops are fully packed, concentric around the root of the original spanning web and can be oriented so as to follow a Manhattan orientation of the underlying grid (as indicated by arrows).

should be related to the exponential convergence of the “monomer-monomer” correlation function to a plateau at large separation (deconfinement), as observed in Ref. [21]. Note finally that a random lattice version of the problem looks particularly promising for obtaining exact results.

ACKNOWLEDGMENTS

We thank M. Bauer, C. Boutillier, F. David, Ph. Di Francesco, B. Duplantier, W. Krauth, J.-M. Luck, and X. Xing for enlightening discussions. The authors acknowledge support from the Geocomp project, ACI Masse de données (E.G.), from the ENRAGE European network, Grant No. MRTN-CT-2004-5616 (E.G. and J.B.) and from the Programme d’Action Intégrée J. Verne “Physical applications of random graph theory” (E.G.). M.B. would like to acknowledge the hospitality of the Service de Physique Théorique of Saclay during the period in which this work was carried out.

APPENDIX A: COULOMB GAS ARGUMENT

Let us present here a heuristic derivation of the relation (3.15) based on a Coulomb gas formulation of the problem. First we note that, as illustrated in Fig. 23, any spanning web configuration with \mathcal{L} loop components can be alternatively coded by a configuration of $2\mathcal{L} + 1$ loops on a square grid dual to the original dimer grid. These loops are such that (i) each loop encloses the root vertex i_0 , (ii) the loops are self- and mutually avoiding and fully packed, i.e., each vertex of the dual grid is visited by a loop, (iii) the loops can be oriented consistently so as to follow a Manhattan orientation on the dual grid. We can relax condition (i) and assign a weight n_0 for each loop that does not enclose i_0 and a weight n for each loop that does enclose i_0 . The correct statistics with a weight y per loop component of the spanning web is then recovered by choosing $n_0 = 0$ and $n = \sqrt{y}$ (and dividing by the residual weight \sqrt{y} associated with the loop around the tree component). The model is expected to lie in the universality class of the dense $O(n_0)$ model which can be described by a

one-dimensional height field.¹ In terms of this height field, the loop model is mapped onto a Coulomb gas model for which various exponents can be obtained exactly [22]. The anomalous weight n for the loops that enclose i_0 is properly accounted for by introducing an electric operator at i_0 with charge q such that $n=2 \cos[\pi(q-u_0)]$. The dimension of such an electric operator is

$$x = \frac{q(q-2u_0)}{2g_0}, \quad (\text{A1})$$

where $n_0=2 \cos(\pi u_0)$ ($0 \leq u_0 \leq 1$), $g_0=1-u_0$, and with the determination of q such that $u_0-1/2 \leq q \leq u_0+1/2$. Here we want $n_0=0$, i.e., $u_0=1/2$ and $n=\sqrt{y}=2 \cos(\pi u)$ with u as in Eq. (3.15), i.e., $q=u+1/2$. We end up with

$$x = u^2 - \frac{1}{4}. \quad (\text{A2})$$

The dimension x of the electric operator measures in particular the algebraic decay as L^{-x} of its average in a finite geometry of linear size L . For a square grid geometry, this average is nothing but the ratio $Z(y; i_0)/Z(0; i_0)$ where the denominator is identified as the partition function of the system in the absence of electric operator. We immediately deduce the relation $x = \gamma(y) - \gamma(0)$, i.e.,

$$\gamma(y) = u^2 - \frac{1}{4} + \gamma(0). \quad (\text{A3})$$

To end the argument and recover Eq. (3.15), we simply rely on a direct calculation of $\gamma(0)=1/2$, as obtained in Ref. [16] from the exact product formula for $Z(0; i_0)=Z_{\text{tree}}$.

APPENDIX B: GENERATING SPANNING WEBS VIA CYCLE POPPING

In this appendix we explain how to generate a random spanning web using a ‘‘cycle-popping’’ algorithm inspired from the Propp-Wilson algorithm for the generation of a random spanning tree. More precisely we extend to random webs the `RANDOMTREEWITHROOT()` procedure explained in Sec. VI of Ref. [18].

Let us begin by recalling how the Propp-Wilson algorithm works in our specific setting. Start with a rectangular grid on which the spanning tree is to be constructed, with the root i_0 at a given position. At each vertex distinct from i_0 , draw a random incident edge uniformly and independently from the other vertices. Pictorially the edge is marked and oriented away from the vertex: a possible outcome of this procedure is illustrated in Fig. 24(a). Note the similarity with the proof of the determinant formula (2.2). By chance, the graph made of the selected edges can be a spanning tree rooted at i_0 (with

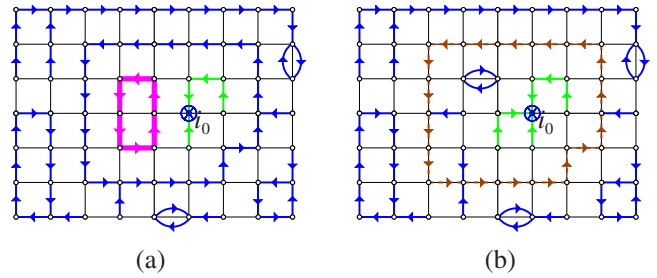


FIG. 24. (Color online) An example of a configuration (a) obtained by drawing at random an edge from each vertex but the root i_0 . A possible configuration (b) obtained from (a) by popping the magenta (thick) cycle. The tree component flowing to i_0 [here in green (light-gray)] can only grow in the process. To generate spanning webs instead of spanning trees, we make all cycles winding around i_0 (such as the brown dashed cycle) unpopable.

edges oriented towards the root), but more likely it will contain one or more (disjoint) cycles (loops) as in Fig. 24(a). Cycle-popping consists in choosing an arbitrary cycle and popping it, i.e., for each vertex on the cycle, drawing a new random outgoing edge uniformly and independently of all previous draws. For instance, Fig. 24(b) shows a possible outcome after the popping of the magenta (thick) cycle in Fig. 24(a). The resulting graph can again contain cycles (some preexisting and some created by popping): in that case repeat the procedure by choosing another cycle and popping it. Otherwise the resulting graph is a spanning tree and the procedure terminates. In Fig. 24, the green (light-gray) edges ‘‘flow’’ to the root, hence they cannot be in a cycle and they must belong to the final tree. One then sees that the green graph can only grow at each step, eventually covering the whole grid.

There are several ways to choose which cycle to pop at each step of the procedure (one could imagine doing it deterministically or randomly), but Propp and Wilson have shown that the actual procedure is (in some precise sense) irrelevant. Furthermore, (i) the procedure terminates almost surely, i.e., only a finite number of cycles have to be popped before none remains and (ii) the resulting spanning tree is a perfect sample of the uniform measure on the set of spanning trees rooted at i_0 . Propp and Wilson actually deal with a slightly more general case, not needed here, and compute bounds on the running time, which establish that this is a very efficient algorithm.

The modification of the algorithm to generate spanning webs is easy. Perform the procedure as before, except that cycles winding around the root i_0 are now considered unpopable and stay in the resulting graph. For instance in Fig. 24(b) the brown (dashed) cycle would be unpopable if we were to generate a spanning web. Only the cycles not winding around the root are popped, until none remains. Propp and Wilson’s analysis (in Sec. VII of Ref. [18]) extends straightforwardly to the case of the unpopable cycles, and we find that (i) the procedure terminates almost surely, and (ii) the resulting graph is now a perfect sample of the uniform measure on graphs (made out of oriented edges, with exactly one edge going out of every vertex, except for the root that has none) whose cycles are all unpopable. One

¹It is known that fully packed loops are in general in a different universality class than dense loops. In particular, on the square lattice, the fully packed loop universality class is described by a three-dimensional height variable. For the model at hand with the extra constraint (iii) above, however, two of the height components are eliminated, leading to an effectively one-dimensional model.

sees easily that such a graph is nothing but a spanning web rooted at i_0 , as defined in Sec. II B, with additional orientations such that each edge not belonging to a cycle “flows” towards the root or an attractor cycle. Since each cycle has two possible orientations that are equally likely, we conclude that the probability to obtain a given unoriented spanning web containing \mathcal{L} loops is $2^{\mathcal{L}}/Z(2, i_0)$, where $Z(2, i_0)$ is the generating function for spanning webs on the grid at hand, rooted at i_0 and counted with a weight $y=2$ per loop, as defined in Eq. (2.4). This is to be contrasted with the weight $y=4$ per loop that arises from the correspondence with dimer configurations with a vacancy, drawn with uniform probability. Knowing the exact bias, it is however straightforward to translate the statistical properties of spanning webs as measured through this algorithm into dimer statistics. Moreover, one can correct the bias directly in the algorithm, at the price

of introducing suitable weights for edges along a seam.

In conclusion, we have provided an algorithm for the generation of random spanning webs belonging to the class of exact or perfect algorithms [18,23]. By the correspondence of Sec. II B, it can be used to simulate dimer configurations on a square lattice with a vacancy. We have not performed a detailed analysis of its efficiency, but we believe it is comparable to the original Propp-Wilson algorithm for rooted spanning trees, and much better than generic CFTP-type algorithms. The comparison with other Monte Carlo algorithms, such as the pivot algorithm [19,20] for the case of periodic boundary conditions is not so clear: typically, these are designed with efficiency in mind, but without an exact knowledge of their “randomness.” Both approaches provide useful and mutually consistent results in our study.

-
- [1] R. H. Fowler and G. S. Rushbrooke, *Trans. Faraday Soc.* **33**, 1272 (1937).
- [2] P. W. Anderson, *Science* **235**, 1196 (1987).
- [3] P. W. Kasteleyn, *Physica (Amsterdam)* **27**, 1209 (1961).
- [4] P. W. Kasteleyn, *J. Math. Phys.* **4**, 287 (1963).
- [5] M. E. Fisher, *Phys. Rev.* **124**, 1664 (1961).
- [6] H. N. V. Temperley and M. E. Fisher, *Philos. Mag.* **6**, 1061 (1961).
- [7] M. E. Fisher and J. Stephenson, *Phys. Rev.* **132**, 1411 (1963).
- [8] B. W. McCoy and T. T. Wu, *The Two-Dimensional Ising Model* (Harvard University Press, Cambridge, MA, 1973).
- [9] R. E. Hartwig, *J. Math. Phys.* **7**, 286 (1966).
- [10] W. J. Tseng and F. Y. Wu, *J. Stat. Phys.* **110**, 671 (2003).
- [11] F. Y. Wu, *Phys. Rev. E* **74**, 020104(R) (2006); **74**, 039907(E) (2006).
- [12] H. N. V. Temperley, in *Combinatorics: Proceedings of the British Combinatorial Conference*, London Mathematical Society Lecture Notes Series No. 13 (Cambridge University Press, Cambridge, 1974) 202.
- [13] R. W. Kenyon, J. G. Propp, and D. B. Wilson, *Electron. J. Comb.* **7**, R25 (2000).
- [14] G. Kirchhoff, *Ann. Phys. Chem.* **72**, 497 (1847).
- [15] N. S. Izmailian, V. B. Priezzhev, and P. Ruelle, *Symmetry, Integr. Geom.: Methods Appl.* **3**, 001 (2007).
- [16] See, for instance, B. Duplantier and F. David, *J. Stat. Phys.* **51**, 327 (1988).
- [17] S. Plouffe, <http://pi.lacim.uqam.ca/>
- [18] J. G. Propp and D. B. Wilson, *J. Algorithms* **27**, 170 (1998).
- [19] W. Krauth and R. Moessner, *Phys. Rev. B* **67**, 064503 (2003).
- [20] W. Krauth, *New Optimization Algorithms in Physics*, edited by A. K. Hartmann and H. Rieger (Wiley-VCH, New York, 2004), Chap. 2.
- [21] P. Fendley, R. Moessner, and S. L. Sondhi, *Phys. Rev. B* **66**, 214513 (2002).
- [22] For an introduction to the Coulomb gas formalism, see B. Nienhuis, *Phase Transitions and Critical Phenomena*, edited by C. Domb and J. L. Lebowitz (Academic Press, New York, 1987).
- [23] See also D. B. Wilson’s online bibliography at <http://research.microsoft.com/~dbwilson/exact>; first published in Vol. 41 of *DIMACS Series in Discrete Mathematics and Theoretical Computer Science* (American Mathematical Society, Providence, RI, 1998).